# Microwave Imaging of Multiple Conducting Cylinders

Chien-Ching Chiu and Yean-Woei Kiang, *Member, IEEE*

*Abstract*—In this paper the inverse scattering for multiple conducting cylinders is investigated. Assume that a plane wave is incident upon separate perfectly conducting cylinders of unknown shapes and the scattered field is measured outside. Using prior knowledge of the rough positions of the scatterers, the shapes of the conducting scatterers can be reconstructed. The Newton–Kantorovitch method is employed to solve nonlinear integral equations and the pseudoinverse technique is used to overcome the ill-posedness. Numerical examples are given to demonstrate the capability of the inversion algorithm. Good reconstruction is obtained even when the multiple scattering between two conductors is serious. In addition, the effect of noise on the reconstruction result is also investigated.

## I. INTRODUCTION

INVERSE scattering of conducting objects has been a subject of interest to researchers for many years. It is applied to many fields of physical science for remotely sensing unknown objects and reconstructing their physical properties. Generally speaking, two kinds of approaches have been developed. The first is an approximate approach. It makes use of the Bojarski identity to reconstruct the shape of a perfectly conducting scatterer [1]–[5]. However, this method requires physical optics approximation. In contrast, the second approach is a rigorous one. It solves the exact equations of the inverse scattering problem by numerical methods [6]–[12]. This technique needs no approximation in formulation, but the calculation is more complex than the approximate approach stated above. Also, this rigorous approach can be further classified into three categories by different physical concepts and numerical techniques.

1) *Newton–Kantorovitch method [6]–[8]:* Roger [6] first, in 1981, applied this method to solving the inverse scattering of a perfectly conducting cylinder by the knowledge of bistatic scattering cross sections. His principal idea is to solve the integral equation by an iterative procedure. Owing to the deficiency of the phase information, the reconstructed result is not satisfactory. Therefore, Kristensson and Vogel [7] used the angular diversity and

least-squares method to overcome the ill-posedness to get a better result in 1986. Later on, Tobocman [8] utilized both angular and frequency diversities to obtain more accurate results.

2) *Colton–Monk method [9]–[11]:* Colton and Monk [9], [10] proposed a novel method, without solving the direct scattering problem, to carry out a series of acoustic wave inverse scattering calculations in 1985 and 1986. This method consists of two steps. The first step solves a boundary value problem in the interior of the unknown scatterer using Herglotz wavefunctions. Then in the second step, the boundary of the scatterer is found as the curve where the boundary condition from the first step is satisfied. They also presented some numerical results for three-dimensional sound-soft impenetrable targets in 1987 [11].

3) *Equivalent source method [12]:* Kirsch and Kress [12] proposed the equivalent source concept to solve the inverse scattering problem. A set of fictitious electric current filaments, of which the amplitudes can be determined by the scattered field, are properly distributed inside the conductor. The scattered field produced by the current filaments and the incident field are summed up and the nodal line that corresponds to the scatterer surface is then reconstructed.

However, the above-mentioned rigorous approaches merely dealt with the object of starlike shape, i.e., an arbitrary point on the surface of a two-dimensional object can be represented in polar coordinates as $(F(\theta), \theta)$, where $F(\theta)$ is a real single-valued function of $\theta$. To our knowledge, there is still no numerical result for the case involving multiple conducting scatterers where the condition of starlike shape is violated.

In this paper the inverse scattering for two separate conducting cylinders in free space, i.e., the case of non-starlike shape, is investigated. We propose an algorithm to reconstruct the shapes of the conducting scatterers by the prior knowledge of the rough locations of the scatterers. The algorithm makes use of the Newton–Kantorovitch method for numerical computation. In Section II, the theoretical formulation for the inverse scattering is presented. We then introduce numerical techniques to solve the integral equations and to overcome the ill-posedness in Section III. Numerical results for reconstructing objects of different shapes and the effect of multiple scattering are discussed in Section IV. Finally, some conclusions are drawn in Section V.

## II. Theoretical Formulation

Let us consider two separate perfectly conducting cylinders with cross section described in polar coordinates in $xy$ plane by the equations $\rho_1 = F_1(\theta_1)$ and $\rho_2 = F_2(\theta_2)$ centered at $(d_1 \cos \psi, d_1 \sin \psi)$ and $(-d_2 \cos \psi, -d_2 \sin \psi)$, respectively, in free space. Let $(\epsilon_0, \mu_0)$ denote the permittivity and permeability respectively of free space. A plane wave whose electric field

$$E_i(F_2(\theta_2) \cos \theta_2 - d_2 \cos \psi, F_2(\theta_2) \sin \theta_2 - d_2 \sin \psi)$$

$$= \int_0^{2\pi} \frac{j}{4} H_0^{(2)}(kr_{04}) J_1(\theta') d\theta'$$

$$+ \int_0^{2\pi} \frac{j}{4} H_0^{(2)}(kr_{02}) J_2(\theta') d\theta' \tag{4}$$

where

$$r_{0i}(\theta_i, \theta') = \sqrt{[F_i(\theta_i) \cos \theta_i - F_i(\theta') \cos \theta']^2 + [F_i(\theta_i) \sin \theta_i - F_i(\theta') \sin \theta']^2}, \quad i = 1, 2$$

$$r_{03}(\theta_1, \theta') = \sqrt{[F_1(\theta_1) \cos \theta_1 - F_2(\theta') \cos \theta' + d \cos \psi]^2 + [F_1(\theta_1) \sin \theta_1 - F_2(\theta') \sin \theta' + d \sin \psi]^2}$$

$$r_{04}(\theta_2, \theta') = \sqrt{[F_2(\theta_2) \cos \theta_2 - F_1(\theta') \cos \theta' - d \cos \psi]^2 + [F_2(\theta_2) \sin \theta_2 - F_1(\theta') \sin \theta' - d \sin \psi]^2}, \quad d = d_1 + d_2.$$

vector is parallel to $z$-axis (i.e., transverse magnetic or TM polarization) is incident upon the scatterers. We assume that the time dependence of the field is harmonic with the factor $\exp(j\omega t)$. Let $\vec{E}_i$ denote the incident field with incident angle $\phi$, as shown in Fig. 1. Then the incident field is given by

$$\vec{E}_i(x, y) = e^{-jk(x \sin \phi + y \cos \phi)} \hat{z}, \qquad k^2 = \omega^2 \epsilon_0 \mu_0. \tag{1}$$

At an arbitrary point $(x, y)$ in Cartesian coordinates outside the scatterers, the scattered field, $\vec{E}_s = \vec{E} - \vec{E}_i$, can be expressed by

$$E_s(x, y) = -\int_0^{2\pi} \frac{j}{4} H_0^{(2)}\left(k\sqrt{(x_1 - F_1(\theta') \cos \theta')^2 + (y_1 - F_1(\theta') \sin \theta')^2}\right) J_1(\theta') d\theta'$$

$$- \int_0^{2\pi} \frac{j}{4} H_0^{(2)}\left(k\sqrt{(x_2 - F_2(\theta') \cos \theta')^2 + (y_2 - F_2(\theta') \sin \theta)^2}\right) J_2(\theta') d\theta' \tag{2}$$

with

$$J_i(\theta_i) = -j\omega\mu_0 \sqrt{F_i^2(\theta_i) + F_i'^2(\theta_i)} \, J_{si}(\theta_i), \quad i = 1, 2$$

$$(x_1, y_1) = (x - d_1 \cos \psi, y - d_1 \sin \psi),$$

$$(x_2, y_2)$$

$$= (x + d_2 \cos \psi, y + d_2 \sin \psi)$$

where $H_0^{(2)}$ is the Hankel function of the second kind of order zero, and $J_{si}(\theta_i)$ is the induced surface current density which is proportional to the normal derivative of electric field on the $i$th conductor surface.

The boundary condition states that the total tangential electric field at the surface of the scatterers must be zero and this yields two integral equations for $J_1(\theta_1)$ and $J_2(\theta_2)$:

$$E_i(F_1(\theta_1) \cos \theta_1 + d_1 \cos \psi, F_1(\theta_1) \sin \theta_1 + d_1 \sin \psi)$$

$$= \int_0^{2\pi} \frac{j}{4} H_0^{(2)}(kr_{01}) J_1(\theta') d\theta'$$

$$+ \int_0^{2\pi} \frac{j}{4} H_0^{(2)}(kr_{03}) J_2(\theta') d\theta', \tag{3}$$

For the direct scattering problem, the scattered field $E_s$ is calculated by assuming that the positions and the shapes of the objects are known. This can be achieved by first solving $J_1$ and $J_2$ in (3) and (4) and calculating $E_s$ in (2).

Next, we consider the following inverse problem: given the scattered field $E_s$ measured outside the scatterers, determine the positions and the shape functions, $F_1(\theta_1)$ and $F_2(\theta_2)$, of the objects. From [5], the approximate centers of the scatterers can be easily found by the Bojarski identity based on the physical optics approximation. Here the details of finding the reference centers of the scatterers are omitted for simplicity. After each center, which in fact can be any point inside each scatterer, is determined, the Newton–Kantorovitch method is then employed to obtain the final shape functions of the scatterers.

First, we define the nonlinear functional systems as

$$h_1(F_1, F_2, J_1, J_2) = E_i(F_1(\theta_1) \cos \theta_1 + d_1 \cos \psi,$$

$$F_1(\theta_1) \sin \theta_1 + d_1 \sin \psi)$$

$$- \int_0^{2\pi} \frac{j}{4} H_0^{(2)}(kr_{01}) J_1(\theta') d\theta'$$

$$- \int_0^{2\pi} \frac{j}{4} H_0^{(2)}(kr_{03}) J_2(\theta') d\theta' \tag{5}$$

$$h_2(F_1, F_2, J_1, J_2) = E_i(F_2(\theta_2) \cos \theta_2 - d_2 \cos \psi,$$

$$F_2(\theta_2) \sin \theta_2 - d_2 \sin \psi)$$

$$- \int_0^{2\pi} \frac{j}{4} H_0^{(2)}(kr_{04}) J_1(\theta') d\theta'$$

$$- \int_0^{2\pi} \frac{j}{4} H_0^{(2)}(kr_{02}) J_2(\theta') d\theta' \tag{6}$$

$$f(F_1, F_2, J_1, J_2) = E_s(x, y) + \int_0^{2\pi} \frac{j}{4} H_0^{(2)}\left(k\sqrt{(x_1 - F_1(\theta') \cos \theta')^2 + (y_1 - F_1(\theta') \sin \theta')^2}\right) J_1(\theta') d\theta'$$

$$+ \int_0^{2\pi} \frac{j}{4} H_0^{(2)}\left(k\sqrt{(x_2 - F_2(\theta') \cos \theta')^2 + (y_2 - F_2(\theta') \sin \theta')^2}\right) J_2(\theta') d\theta' \tag{7}$$

and let symbols $\delta h_1$, $\delta h_2$, and $\delta f$ denote variations of the quantities $h_1$, $h_2$, and $f$, respectively, due to small variations of $\delta F_1$, $\delta F_2$, $\delta J_1$ and $\delta J_2$. By differentiating (5), (6), and (7), one obtains

$$\delta h_1(F_1, F_2, J_1, J_2)$$

$$= (-jk)(\cos \theta_1 \sin \phi + \sin \theta_1 \cos \phi)$$

$$\cdot E_i(F_1(\theta_1) \cos \theta_1 + d_1 \cos \psi, F_1(\theta_1) \sin \theta_1$$

$$+ d_1 \sin \psi) \delta F_1(\theta_1)$$

$$- \int_0^{2\pi} \delta\left[\frac{j}{4} H_0^{(2)}(kr_{01})\right] J_1(\theta') d\theta'$$

$$- \int_0^{2\pi} \delta\left[\frac{j}{4} H_0^{(2)}(kr_{03})\right] J_2(\theta') d\theta'$$

$$- \int_0^{2\pi} \frac{j}{4} H_0^{(2)}(kr_{01}) \delta J_1(\theta') d\theta'$$

$$- \int_0^{2\pi} \frac{j}{4} H_0^{(2)}(kr_{03}) \delta J_2(\theta') d\theta' \qquad (8)$$

$$\delta h_2(F_1, F_2, J_1, J_2)$$

$$= (-jk)(\cos \theta_2 \sin \phi + \sin \theta_2 \cos \phi)$$

$$\cdot E_i(F_2(\theta_2) \cos \theta_2 - d_2 \cos \psi, F_2(\theta_2) \sin \theta_2$$

$$- d_2 \sin \psi) \delta F_2(\theta_2)$$

$$- \int_0^{2\pi} \delta\left[\frac{j}{4} H_0^{(2)}(kr_{04})\right] J_1(\theta') d\theta'$$

$$- \int_0^{2\pi} \delta\left[\frac{j}{4} H_0^{(2)}(kr_{02})\right] J_2(\theta') d\theta'$$

$$- \int_0^{2\pi} \frac{j}{4} H_0^{(2)}(kr_{04}) \delta J_1(\theta') d\theta'$$

$$- \int_0^{2\pi} \frac{j}{4} H_0^{(2)}(kr_{02}) \delta J_2(\theta') d\theta' \qquad (9)$$

$$\delta f(F_1, F_2, J_1, J_2) = \int_0^{2\pi} \delta\left\{\frac{j}{4} H_0^{(2)}\left(k\sqrt{(x_1 - F_1(\theta') \cos \theta')^2 + (y_1 - F_1(\theta') \sin \theta')^2}\right)\right\} J_1(\theta') d\theta'$$

$$+ \int_0^{2\pi} \delta\left\{\frac{j}{4} H_0^{(2)}\left(k\sqrt{(x_2 - F_2(\theta') \cos \theta')^2 + (y_2 - F_2(\theta') \sin \theta')^2}\right)\right\} J_2(\theta') d\theta'$$

$$+ \int_0^{2\pi} \frac{j}{4} H_0^{(2)}\left(k\sqrt{(x_1 - F_1(\theta') \cos \theta')^2 + (y_1 - F_1(\theta') \sin \theta')^2}\right) \delta J_1(\theta') d\theta'$$

$$+ \int_0^{2\pi} \frac{j}{4} H_0^{(2)}\left(k\sqrt{(x_2 - F_2(\theta') \cos \theta')^2 + (y_2 - F_2(\theta') \sin \theta')^2}\right) \delta J_2(\theta') d\theta' \qquad (10)$$

where

$$\delta\left[\frac{j}{4} H_0^{(2)}(kr_{0i})\right] = \frac{-jk}{4}\left[\frac{F_i(\theta_i) - F_i(\theta') \cos(\theta_i - \theta')}{r_{0i}} \delta F_i(\theta_i) + \frac{F_i(\theta') - F_i(\theta_i) \cos(\theta_i - \theta')}{r_{0i}} \delta F_i(\theta')\right]$$

$$\cdot H_1^{(2)}(kr_{0i}), \qquad i = 1, 2$$

$$\delta\left[\frac{j}{4} H_0^{(2)}(kr_{03})\right] = \frac{-jk}{4}\left[\frac{F_1(\theta_1) - F_2(\theta') \cos(\theta_1 - \theta') + d\cos(\psi - \theta_1)}{r_{03}} \delta F_1(\theta_1)\right.$$

$$\left. + \frac{F_2(\theta') - F_1(\theta_1) \cos(\theta_1 - \theta') - d\cos(\psi - \theta_1)}{r_{03}} \delta F_2(\theta')\right] H_1^{(2)}(kr_{03})$$

$$\delta\left[\frac{j}{4} H_0^{(2)}(kr_{04})\right] = \frac{-jk}{4}\left[\frac{F_2(\theta_2) - F_1(\theta') \cos(\theta_2 - \theta') - d\cos(\psi - \theta_2)}{r_{04}} \delta F_2(\theta_2)\right.$$

$$\left. + \frac{F_1(\theta') - F_2(\theta_2) \cos(\theta_2 - \theta') + d\cos(\psi - \theta_2)}{r_{04}} \delta F_1(\theta')\right] H_1^{(2)}(kr_{04})$$

$$\delta\left\{\frac{j}{4} H_0^{(2)}\left(k\sqrt{(x_i - F_i(\theta') \cos \theta')^2 + (y_i - F_i(\theta') \sin \theta')^2}\right)\right\}$$

$$= \frac{-jk}{4}\left(\frac{F_i(\theta') - (x_i \cos \theta' + y_i \sin \theta')}{\sqrt{(x_i - F_i(\theta') \cos \theta')^2 + (y_i - F_i(\theta') \sin \theta')^2}} \delta F_i(\theta')\right)$$

$$\cdot H_1^{(2)}\left(k\sqrt{(x_i - F_i(\theta') \cos \theta')^2 + (y_i - F_i(\theta') \sin \theta')^2}\right), \qquad i = 1, 2.$$

To satisfy the boundary condition, $\delta h_1$ and $\delta h_2$ are set to zero. By using the least-squares method to solve (8), (9), and (10), one obtains the differential increments of the shape functions in each iteration. Then we can solve this inverse problem accordingly by an iterative procedure.

### III. COMPUTATIONAL TECHNIQUE

For numerical calculation of the direct problem, we use the moment method [13], [14] to solve (3), (4), and (2) with pulse basis functions $\{P_n(\theta)\}$ for expanding and Dirac delta functions for testing. Let

$$J_i(\theta_i) \simeq \sum_{n=1}^{M_d} B_{in} P_n(\theta_i), \qquad i = 1, 2$$

Then (3) and (4) can be transformed into a matrix equation

$$E_i(F_1(\theta_m)\cos\theta_m + d_1\cos\psi, F_1(\theta_m)\sin\theta_m + d_1\sin\psi)$$

$$= \sum_{n=1}^{M_d} (\hat{L}_1)_{mn} \cdot B_{1n} + \sum_{n=1}^{M_d} (\hat{L}_3)_{mn} \cdot B_{2n}$$

$$E_i(F_2(\theta_m)\cos\theta_m - d_2\cos\psi, F_2(\theta_m)\sin\theta_m - d_2\sin\psi)$$

$$= \sum_{n=1}^{M_d} (\hat{L}_4)_{mn} \cdot B_{1n} + \sum_{n=1}^{M_d} (\hat{L}_2)_{mn} \cdot B_{2n}$$

where

$$(\hat{L}_i)_{mn} = \int_{\Delta C_n} \frac{j}{4} H_0^{(2)}(kr_{0i}(\theta_m, \theta')) d\theta', \qquad i = 1, 2, 3, 4$$

and $\Delta C_i$ is the $i$th segment of the scatterer contour from $\theta = 2\pi(i-1)/M_d$ to $\theta = 2\pi i/M_d$. Note that the regularization procedure is hidden in the truncation of series expansion of $J$. Also (2) becomes

calculation. For convenience, a vector $\vec{F}$ is defined by

$$(\vec{F})_i = \begin{cases} (\vec{F}_1)_i, & 0 \le i \le N \\ (\vec{F}_2)_{i-(N+1)}, & N+1 \le i \le 2N+1 \end{cases}$$

$$(\vec{F}_i)_j = \begin{cases} (A_i)_j, & 0 \le j \le N/2 \\ (A_i')_{j-N/2}, & N/2+1 \le j \le N \end{cases} \quad i = 1, 2.$$

By point-matching technique [14], (8), (9), and (10) can be cast into matrix form as

$$\delta\vec{h}_1 = \hat{S} \cdot \delta\vec{F} + \hat{U}_1 \cdot \delta\vec{B}_1 + \hat{U}_3 \cdot \delta\vec{B}_2 \qquad (11)$$

$$\delta\vec{h}_2 = \hat{\hat{S}} \cdot \delta\vec{F} + \hat{U}_4 \cdot \delta\vec{B}_1 + \hat{U}_2 \cdot \delta\vec{B}_2 \qquad (12)$$

$$\delta\vec{f} = \hat{C} \cdot \delta\vec{F} + \hat{T}_1 \cdot \delta\vec{B}_1 + \hat{T}_2 \cdot \delta\vec{B}_2 \qquad (13)$$

where

$$(\delta\vec{F})_i = \begin{cases} \delta(\vec{F}_1)_i, & 0 \le i \le N \\ \delta(\vec{F}_2)_{i-(N+1)}, & N+1 \le i \le 2N+1 \end{cases}$$

$$(\delta\vec{B}_i)_j = \delta(B_i)_j, \quad 1 \le j \le M, i = 1, 2$$

$$\hat{S} = [[\hat{S}_1], [\hat{S}_2]]$$

$$(\hat{S}_k)_{ij} = \begin{cases} (S_k)_{ij}, & 1 \le i \le M, 0 \le j \le N/2 \\ (S_k')_{ij-N/2}, & 1 \le i \le M, N/2+1 \le j \le N \end{cases}$$

$$k = 1, 2$$

$$E_s(x, y) = -\sum_{n=1}^{M_d} B_{1n} \int_{\Delta C_n} \frac{j}{4} H_0^{(2)} \left( k\sqrt{(x_1 - F_1(\theta')\cos\theta')^2 + (y_1 - F_1(\theta')\sin\theta')^2} \right) d\theta'$$

$$- \sum_{n=1}^{M_d} B_{2n} \int_{\Delta C_n} \frac{j}{4} H_0^{(2)} \left( k\sqrt{(x_2 - F_2(\theta')\cos\theta')^2 + (y_2 - F_2(\theta')\sin\theta')^2} \right) d\theta'.$$

To solve (8), (9), and (10) for the inverse problem, we choose the following expansions:

$$F_i(\theta_i) \simeq \sum_{n=0}^{N/2} A_{in}\cos(n\theta_i) + \sum_{n=1}^{N/2} A_{in}'\sin(n\theta_i), \qquad i = 1, 2$$

$$J_i(\theta_i) \simeq \sum_{n=1}^{M} B_{in} P_n(\theta_i), \qquad i = 1, 2$$

where $A_{in}$ and $A_{in}'$ are real numbers, and $B_{in}$ are complex in general. Note that $M$ must be different from $M_d$, since it is crucial that the synthetic data generated through a forward solver are not alike to those obtained by the inverse solver. In general, $M_d$ is chosen to be $2M$ in our

$$\hat{\hat{S}} = [[\hat{\hat{S}}_1], [\hat{\hat{S}}_2]]$$

$$(\hat{\hat{S}}_k)_{ij} = \begin{cases} (\bar{S}_k)_{ij}, & 1 \le i \le M, 0 \le j \le N/2 \\ (\bar{S}_k')_{ij-N/2}, & 1 \le i \le M, N/2+1 \le j \le N \end{cases}$$

$$k = 1, 2$$

$$(\hat{U}_k)_{ij} = (U_k)_{ij}, \quad 1 \le i \le M, 1 \le j \le M, k = 1, 2, 3, 4$$

$$\hat{C} = [[\hat{C}_1], [\hat{C}_2]]$$

$$(\hat{C}_k)_{ij} = \begin{cases} (C_k)_{ij}, & 1 \le i \le M', 0 \le j \le N/2 \\ (C_k')_{ij-N/2}, & 1 \le i \le M', N/2+1 \le j \le N \end{cases}$$

$$k = 1, 2$$

$$(\hat{T}_k)_{ij} = (T_k)_{ij}, \quad 1 \le i \le M', 1 \le j \le M, k = 1, 2$$

where $M'$ is the number of points for measuring the scattered field. $(S_1)_{mn}$, $(S_1')_{mn}$, $(S_2)_{mn}$, $(S_2')_{mn}$, $(\overline{S}_1)_{mn}$, $(\overline{S}_1')_{mn}$, $(\overline{S}_2)_{mn}$, $(\overline{S}_2')_{mn}$, $(U_1)_{mn}$, $(U_2)_{mn}$, $(U_3)_{mn}$, $(U_4)_{mn}$, $(C_1)_{mn}$, $(C_1')_{mn}$, $(C_2)_{mn}$, $(C_2')_{mn}$, $(T_1)_{mn}$ and $(T_2)_{mn}$ are appropriate coefficients that can be obtained by tedious mathematical manipulations (see Appendix).

To satisfy the boundary condition, we set $\delta \vec{h}_1 = 0$ and $\delta \vec{h}_2 = 0$. After eliminating $\delta \vec{B}_1$ and $\delta \vec{B}_2$ in (13), we get

$$
\begin{aligned}
\delta \vec{f} = & \left\{ \hat{C} + \hat{T}_1 \cdot \left[ \hat{U}_1 - \hat{U}_3 \cdot \left( \hat{U}_2 \right)^{-1} \cdot \hat{U}_4 \right]^{-1} \right. \\
& \cdot \left[ \hat{U}_3 \cdot \left( \hat{U}_2 \right)^{-1} \cdot \hat{\vec{S}} - \hat{S} \right] - \hat{T}_2 \cdot \left( \hat{U}_2 \right)^{-1} \\
& \cdot \left[ \hat{\vec{S}} + \hat{U}_4 \cdot \left[ \hat{U}_1 - \hat{U}_3 \cdot \left( \hat{U}_2 \right)^{-1} \right. \right. \\
& \left. \left. \left. \cdot \hat{U}_4 \right]^{-1} \cdot \left[ \hat{U}_3 \cdot \left( \hat{U}_2 \right)^{-1} \cdot \hat{\vec{S}} - \hat{S} \right] \right] \right\} \cdot \delta \vec{F} \\
\triangleq & \ \hat{D} \cdot \delta \vec{F}. 
\end{aligned} \tag{14}
$$

Although (14) is valid only for a single incoming wave, one can generalize it to the case of incoming waves of multi-incident angles easily. Note that the matrix $\hat{D}$ in (14) is usually a nonsquare one. Furthermore, (14) derived from the integral equation of electromagnetic scattering is usually ill posed. In order to find an adequate solution for (14), the regularization is needed. In the regularization procedure, instead of solving (14) directly, we can solve an optimization problem which minimizes the functional defined as

$$
\| \text{Re} \left[ \hat{D}^\dagger \cdot \hat{D} \right] \cdot \delta \vec{F} + \text{Re} \left[ \hat{D}^\dagger \cdot \vec{f} \right] \| \tag{15a}
$$

with the constraint

$$
\| \delta \vec{F} \| \text{ is minimum} \tag{15b}
$$

where $\| \cdot \|$ denotes the norm, the dagger denotes transpose and complex conjugate, and Re means taking the real part. Since the elements of $\delta \vec{F}$ are real quantities, we take the real parts of $\hat{D}^\dagger \cdot \hat{D}$ and $\hat{D}^\dagger \cdot \vec{f}$. Then (15) is solved by means of a pseudo-inverse algorithm [13], which is based on the Gram–Schmidt orthogonalization. The pseudoinverse transformation circumvents numerical instability inherent to inverse scattering and generates a unique solution for (15). The minimization of $\| \delta \vec{F} \|$ can be somewhat interpreted as the smoothness requirement for the boundary of the scatterers. Therefore, the condition of (15) is the minimization of the least-square error between the measured field and the calculated field with the constraint of a smooth boundary. In reality, the matrix $\text{Re}(\hat{D}^\dagger \cdot \hat{D})$ is not absolutely singular. However, in order to find the pseudoinverse solution of (15), one has to set some of its column vectors as linearly dependent. In our calculation, the number of dependent columns is so chosen as to minimize the difference between the measured field and the calculated field in the least-squares sense in each iteration.

During the implementation of the iterative procedure, we first choose the initial guess $(\vec{F})^0$ and solve for $(\delta \vec{F})^k$ in (15) to obtain $(\vec{F})^{k+1} = (\vec{F})^k + (\delta \vec{F})^k$, $k = 0, 1, 2, 3 \cdots$. Iteration continues until convergence is achieved. To monitor convergence, after each iteration the calculated profile $F_i^{\text{cal}}(\theta_i)$ is substituted into (3), (4), and (2) to produce the calculated scattered field $E_s^{\text{cal}}(\vec{r})$ and the discrepancy

$$
\text{DF} = \left\{ \frac{1}{M_t'} \sum_{m=1}^{M_t'} |E_2^{\text{exp}}(\vec{r}_m) - E_s^{\text{cal}}(\vec{r}_m)|^2 / |E_s^{\text{exp}}(\vec{r}_m)|^2 \right\}^{1/2}
$$

is determined, where $M_t'$ is the total number of measurement points and $E_s^{\text{exp}}$ the measured scattered field. Iteration will be stopped when either DF changes by less than 4% in two successive iterations or DF is smaller than $5 \times 10^{-5}$ in two successive iterations.

## IV. NUMERICAL RESULTS

By numerical simulation we illustrate the performance of the proposed inversion algorithm and its sensitivity to random error in the scattered field. Let us consider two separate perfectly conducting cylinders in free space and a plane wave of unit amplitude is incident upon the objects, as shown in Fig. 1. The frequency of the incident electromagnetic wave is chosen to be 3 GHz, i.e., the wavelength $\lambda$ is 0.1 m. In the examples the size of the scatterer is about one-third the wavelength, so the frequency is in the resonance range.

In our simulation three different examples are considered. To reconstruct the shapes of the cylinders, the objects are illuminated by four incident waves with incident angles $\phi = 0°$, $90°$, $180°$, and $270°$, and the measurement is taken on a circle of radius $R'$ at equal spacing. In our cases, $R'$ is chosen much larger than $2D'^2/\lambda$ corresponding to the far-field measurement, where $D'$ is the largest dimension of the scatterer. Note that for each incident angle, eight measurement points at equal spacing are used, and there are totally 32 measurement points in each simulation. Of course, the measured scattered field is computed numerically by the moment method. The number of unknowns is set to 14 (i.e., $2N + 2 = 14$) and $M$ is set to 30.

In the first example, both $d_1$ and $d_2$ are set to 0.05 m and $\psi$ is $0°$. The two shape functions are chosen to be $F_1(\theta_1) = 0.03$ m and $F_2(\theta_2) = 0.03$ m, respectively. The measurement radius $R'$ is chosen to be 7 m. In order to investigate the multiple scattering effect, the first-order scattered field and total scattered field for the incident angle $\phi = 90°$ are plotted in Fig. 2. Here the first-order scattered field is the sum of the scattered field due to each scatterer in the absence of the other one. The total scattered field corresponds to the whole scattering from the two coexistent scatterers including multiple scattering effect. Note that the difference between the first-order and total scattered fields in the root mean square (rms)
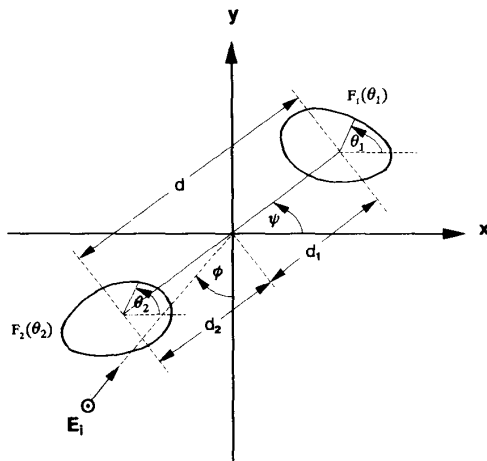
Fig. 1.   Geometry of the problem in the $(x, y)$ plane.



(a)



(b)
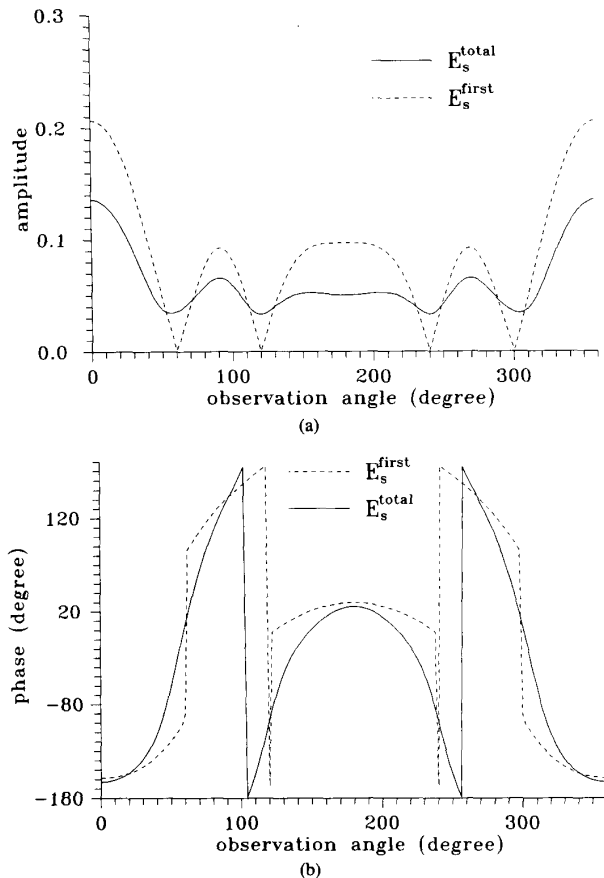
Fig. 2.   First-order and total scattered fields for the incident angle $\phi = 90°$. (a) Amplitude. (b) Phase.

sense is about 65%, i.e.,

$$\left\{ \frac{1}{M_1} \sum_{m=1}^{M_1} |E_s^{\text{first}}(\vec{r}_m) \right.$$

$$\left. - E_s^{\text{total}}(\vec{r}_m)|^2 / |E_s^{\text{total}}(\vec{r}_m)|^2 \right\}^{1/2} \approx 0.65$$

where $M_1$ is set to 180. It is obvious that multiple scattering effect is serious owing to the short distance between these two conductors. The reconstructed shape functions are plotted in Fig. 3. It is seen that the reconstruction is fine enough except on the facing portions of the two objects. This is due to the fact that those portions are not directly illuminated by the incident wave and serious multiple scattering effect occurs there. However, the relative reconstruction error is still very small and it is, for each scatterer, about $1 \times 10^{-2}$ in the rms sense. Here the relative reconstruction error for the $i$th scatterer is defined as

$$\left\{ \frac{1}{M_2} \sum_{m=1}^{M_2} \left[ F_i^{\text{cal}}(\theta_m) - F_i(\theta_m) \right]^2 / [F_i(\theta_m)]^2 \right\}^{1/2}$$

where $M_2$ is set to 60. The good reconstruction result can be explained by the fact that our inversion algorithm has exactly taken multiple scattering effect into account. Viewing from this aspect, we may deduce that the Bojarski identity or the diffraction tomography, which considers only the first-order scattering, cannot obtain the same high image quality as ours in the presence of serious multiple scattering. In addition, we also see that the adjustment of the two shape functions is almost the same in the iteration process due to the symmetrical property.

For investigating the effect of noise, we add to each complex scattered field $E_s(\vec{r})$ a quantity $b + cj$ where $b$ and $c$ are independent random numbers having a uniform distribution over 0 to the noise level times the rms value of scattered field. The noise levels applied include $10^{-3}$, $10^{-2}$, $5 \times 10^{-2}$, $10^{-1}$, $2 \times 10^{-1}$ and $4 \times 10^{-1}$. The relative reconstruction errors are shown in Fig. 4. It shows that the effect of noise is tolerable for noise levels below $10^{-1}$.

Now, we choose a distance of $d_1 = d_2 = 0.5$ m, instead of $d_1 = d_2 = 0.05$ m as in the previous example, to investigate the effect of the separation distance between scatterers on the reconstruction result. Satisfactory results are plotted in Fig. 5. Note that the reconstruction result of the last iteration cannot be distinguished from the exact one by the naked eye. Comparing Fig. 3 with Fig. 5, we find out that the reconstruction is better in the case of large separation. Physically this can be explained by the fact that multiple scattering effect decreases as the separation distance between two conductors increases. In other words, the reconstruction results become better owing to the lesser multiple scattering effect.

In the second example, the shape functions are chosen as $F_1(\theta_1) = (0.026 - 0.009 \cos(2\theta_1))$m and $F_2(\theta_2) =$
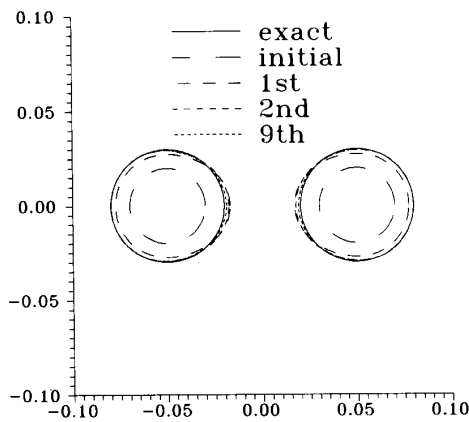
Fig. 3. Shape functions for example 1 with $d_1 = d_2 = 0.05$ m. The solid curve represents the exact shape, while the dashed curves are calculated shapes in iteration process.
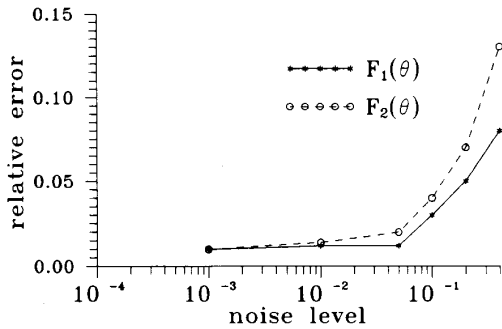


Fig. 4. Relative error for each scatterer in example 1 as a function of noise level.
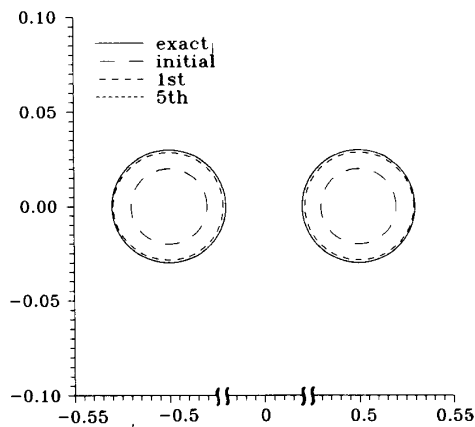


Fig. 5. Shape functions for example 1 with $d_1 = d_2 = 0.5$ m. The solid curve represents the exact shape, while the dashed curves are calculated shapes in iteration process.
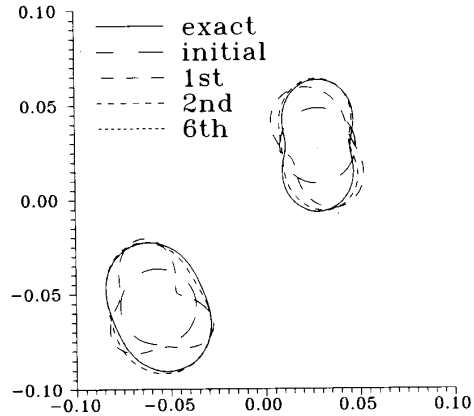


Fig. 6. Shape functions for example 2. The solid curve represents the exact shape, while the dashed curves are calculated shapes in iteration process.

$(0.03 - 0.0035 \cos(2\theta_2) - 0.0035 \sin(2\theta_2))$ m. The parameters $R'$, $\psi$, $d_1$ and $d_2$ are chosen as 7 m, 45°, 0.04 m and 0.08 m respectively. The purpose of this example is to show that our method is able to reconstruct the scatterers which are not symmetrically located about either the $x$-axis or the $y$-axis. Satisfactory results are shown in Fig. 6. The relative error for each scatterer is less than 1%.

In the third example, the shape functions are selected to be $F_1(\theta_1) = (0.03 + 0.0025 \cos \theta_1 - 0.005 \cos(2\theta_1) + 0.005 \cos(3\theta_1))$ m and $F_2(\theta_2) = (0.03 + 0.005 \sin(3\theta_2))$ m. The parameters $R'$, $\psi$, $d_1$ and $d_2$ are chosen as 7 m, 135°, 0.08 m and 0.07 m, respectively. Note that the scatterers are now located in the second and fourth quadrants. This example has further verified the reliability of our algorithm. Refer to Fig. 7 for details. The relative error is about 1% for each scatterer.

From the above three example, we can conclude that our imaging or inverse scattering algorithm is accurate and can be implemented numerically.

## V. CONCLUSION

We have proposed an algorithm for reconstructing the shapes of two perfectly conducting objects by the knowledge of scattered field. The approximate centers of the scatterers can be obtained by the Bojarski identity, and the Newton-Kantorovitch algorithm and moment method have been used to transform the nonlinear integral equations into matrix forms. Then these matrix equations are solved by the pseudoinverse transformation to obtain a stable approximate solution. By means of the above numerical techniques, good reconstruction is obtained from the simulated scattered field either with or without additive random noise. Numerical results have also demonstrated that the reconstruction result is still quite good even when the multiple scattering between scatterers is serious.
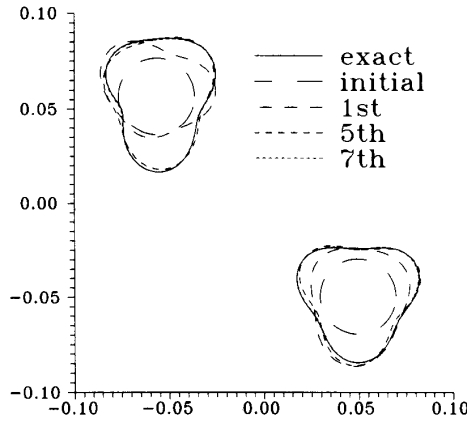
Fig. 7. Shape functions for example 3. The solid curve represents the exact shape, while the dashed curves are calculated shapes in iteration process.

## APPENDIX

Given in the following are some of the matrix elements in (11), (12), and (13)

where

$$(x_{1m}, y_{1m}) = (x_m - d_1 \cos \psi, y_m + d_1 \sin \psi),$$

$$(x_{2n}, y_{2m}) = (x_m + d_2 \cos \psi, y_m + d_2 \sin \psi).$$

Here the symbol PV denotes the Cauchy principal value. Indeed, the corresponding integrals have singularities of the form $1/(\theta - \theta')$ when $\theta \to \theta'$, and thus these types of integrals are evaluated as Cauchy principal values. Note that the elements of the matrices $S_1'$, $S_2'$, $\bar{S}_1'$, $\bar{S}_2'$, $C_1'$ and $C_2'$ can also be derived similarly.

## REFERENCES

[1] R. M. Lewis, "Physical optics inverse diffraction," *IEEE Trans. Antennas Propagat.*, vol. AP-17, pp. 308–314, May 1969.
[2] W. Tabbara, "On an inverse scattering method," *IEEE Trans. Antennas Propagat.*, vol. AP-21, pp. 245–247, Mar. 1973.
[3] C. K. Chan and N. H. Farhat, "Frequency swept tomographic imaging of three dimensional perfectly conducting objects," *IEEE Trans. Antennas Propagat.*, vol AP-29, pp. 312–319, Mar. 1981.

$$(S_1)_{mn} = (-jk)(\cos \theta_m \sin \phi + \sin \theta_m \cos \phi) E_i(F_1(\theta_m) \cos \theta_m + d_1 \cos \psi, F_1(\theta_m) \sin \theta_m + d_1 \sin \psi) \cos(n\theta_m)$$

$$+ \text{PV} \int_0^{2\pi} \frac{jk}{4} \frac{F_1(\theta_m) - F_1(\theta') \cos(\theta_m - \theta')}{r_{01}(\theta_m, \theta')} H_1^{(2)}(kr_{01}(\theta_m, \theta')) \cos(n\theta_m) J_1(\theta') d\theta'$$

$$+ \text{PV} \int_0^{2\pi} \frac{jk}{4} \frac{F_1(\theta') - F_1(\theta_m) \cos(\theta_m - \theta')}{r_{01}(\theta_m, \theta')} H_1^{(2)}(kr_{01}(\theta_m, \theta')) \cos(n\theta') J_1(\theta') d\theta'$$

$$+ \int_0^{2\pi} \frac{jk}{4} \frac{F_1(\theta_m) - F_2(\theta') \cos(\theta_m - \theta') + d \cos(\psi - \theta_m)}{r_{03}(\theta_m, \theta')} H_1^{(2)}(kr_{03}(\theta_m, \theta')) \cos(n\theta_m) J_2(\theta') d\theta'$$

$$(S_2)_{mn} = \int_0^{2\pi} \frac{jk}{4} \frac{F_2(\theta') - F_1(\theta_m) \cos(\theta_m - \theta') - d \cos(\psi - \theta_m)}{r_{03}(\theta_m, \theta')} H_1^{(2)}(kr_{03}(\theta_m, \theta')) \cos(n\theta') J_2(\theta') d\theta'$$

$$(\bar{S}_1)_{mn} = \int_0^{2\pi} \frac{jk}{4} \frac{F_1(\theta') - F_2(\theta_m) \cos(\theta_m - \theta') + d \cos(\psi - \theta_m)}{r_{04}(\theta_m, \theta')} H_1^{(2)}(kr_{04}(\theta_m, \theta')) \cos(n\theta') J_1(\theta') d\theta'$$

$$(\bar{S}_2)_{mn} = (-jk)(\cos \theta_m \sin \phi + \sin \theta_m \cos \phi) E_i(F_2(\theta_m) \cos \theta_m - d_2 \cos \psi, F_2(\theta_m) \sin \theta_m - d_2 \sin \psi) \cos(n\theta_m)$$

$$+ \text{PV} \int_0^{2\pi} \frac{jk}{4} \frac{F_2(\theta_m) - F_2(\theta') \cos(\theta_m - \theta')}{r_{02}(\theta_m, \theta')} H_1^{(2)}(kr_{02}(\theta_m, \theta')) \cos(n\theta_m) J_2(\theta') d\theta'$$

$$+ \text{PV} \int_0^{2\pi} \frac{jk}{4} \frac{F_2(\theta') - F_2(\theta_m) \cos(\theta_m - \theta')}{r_{02}(\theta_m, \theta')} H_1^{(2)}(kr_{02}(\theta_m, \theta')) \cos(n\theta') J_2(\theta') d\theta'$$

$$+ \int_0^{2\pi} \frac{jk}{4} \frac{F_2(\theta_m) - F_1(\theta') \cos(\theta_m - \theta') - d \cos(\psi - \theta_m)}{r_{04}(\theta_m, \theta')} H_1^{(2)}(kr_{04}(\theta_m, \theta')) \cos(n\theta_m) J_1(\theta') d\theta'$$

$$(U_i)_{mn} = -\int_{\Delta C_n} \frac{j}{4} H_0^{(2)}(kr_{0i}(\theta_m, \theta')) d\theta', \qquad i = 1, 2, 3, 4$$

$$(C_i)_{mn} = \int_0^{2\pi} \frac{-jk}{4} \frac{F_i(\theta') - (x_{im} \cos \theta' + y_{im} \sin \theta')}{\sqrt{(x_{im} - F_i(\theta') \cos \theta')^2 + (y_{im} - F_i(\theta') \sin \theta')^2}}$$

$$\cdot H_1^{(2)}\left(k\sqrt{(x_{im} - F_i(\theta') \cos \theta')^2 + (y_{im} - F_i(\theta') \sin \theta')^2}\right) \cos(n\theta') J_i(\theta') d\theta', \qquad i = 1, 2$$

$$(T_i)_{mn} = \int_{\Delta c_n} \frac{j}{4} H_0^{(2)}\left(k\sqrt{(x_{im} - F_i(\theta') \cos \theta')^2 + (y_{im} - F_i(\theta') \sin \theta')^2}\right) d\theta', \qquad i = 1, 2$$

[4] N. N. Bojarski, "A survey of the physical optics inverse scattering identity," *IEEE Trans. Antennas Propagat.*, vol. AP-30, pp. 980–989, Sept. 1982.

[5] T. H. Chu and N. H. Farhat, "Polarization effects in microwave diversity imaging of perfectly conducting cylinders," *IEEE Trans. Antennas Propagat.*, vol. 37, pp. 235–244, Feb. 1989.

[6] A. Roger, "Newton–Kantorovitch algorithm applied to an electromagnetic inverse problem," *IEEE Trans. Antennas Propagat.*, vol. AP-29, pp. 232–238, Mar. 1981.

[7] G. Kristensson and C. R. Vogel, "Inverse problems for acoustic waves using the penalised likelihood method," *Inverse Problems*, vol. 2, pp. 461–479, Nov. 1986.

[8] W. Tobocman, "Inverse acoustic wave scattering in two dimensions from impenetrable targets," *Inverse Problems*, vol. 5, pp. 1131–1144, Dec. 1989.

[9] D. Colton and P. Monk, "A novel method for solving the inverse scattering problem for time-harmonic acoustic waves in the resonance region," *SIAM J. Appl. Math.*, vol. 45, pp. 1039–1053, Dec. 1985.

[10] ——, "A novel method for solving the inverse scattering problem for time-harmonic acoustic waves in the resonance region II, " *SIAM J. Appl. Math.*, vol. 46, pp. 506–523, June 1986.

[11] ——, "The numerical solution of the three-dimensional inverse scattering problem for time-harmonic acoustic waves," *SIAM J. Sci. Stat. Comput.*, vol. 8, pp. 278–291, May 1987.

[12] A. Kirsch, R. Kress, P. Monk and A. Zinn, "Two methods for solving the inverse acoustic scattering problem," *Inverse Problems*, vol. 4, pp. 749–770, Aug. 1988.

[13] M. M. Ney, "Method of moments as applied to electromagnetic problem," *IEEE Trans. Microwave Theory Tech.*, vol. MTT-33, pp. 972–980, Oct. 1985.

[14] R. F. Harrington, *Field Computation by Moment Methods.* New York: Macmillan, 1968.

**Chien-Ching Chiu** was born in Taoyuan, Taiwan, Republic of China, on January 23, 1963. He received the B.S.C.E. degree from National Chiao Tung University, Hsinchu, Taiwan, in 1985 and the M.S.E.E. and Ph.D. degrees from National Taiwan University, Taipei, Taiwan, in 1987 and 1991 respectively.

From 1987 to 1989, he served in the ROC Army Force as a communication officer. In 1992 he joined the faculty of the Department of Electronic Engineering, Tamkang University, where he is now an Associate Professor. His current research interests include microwave imaging and numerical techniques in electromagnetics.

**Yean-Woei Kiang** (S'81–M'84) was born in Panchiao, Taiwan, Republic of China, on October 27, 1954. He received the B.S.E.E., M.S.E.E., and Ph.D. degrees from National Taiwan University, Taipei, Taiwan, in 1977, 1979, and 1984, respectively.

In 1979 he joined the faculty of the Department of Electrical Engineering, National Taiwan University, where he is now a Professor. From 1982 to 1984, he was a Visiting Scholar at the Department of Electrical Engineering, University of Illinois, Urbana. His research interests include wave propagation, scattering, inverse scattering, and target discrimination.